IEEE Open Journal of Nanotechnology

Received 22 September 2022; revised 3 November 2022; accepted 7 November 2022. Date of publication 10 November 2022; date of current version 22 December 2022. The review of this article was arranged by Associate Editor James Morris.

Digital Object Identifier 10.1109/OJNANO.2022.3221141

Modeling and Analysis of Cu-Carbon Nanotube Composites for Sub-Threshold Interconnects

ASHISH SINGH [1], BRAJESH KUMAR KAUSHIK [2] (Senior Member, IEEE), AND ROHIT DHIMAN [1] (Member, IEEE)

[1]Electronics and Communication Engineering Department, National Institute of Technology, Hamirpur, HP 177 005, India
[2]Electronics and Communication Engineering Department, Indian Institute of Technology Roorkee, Roorkee, UK 247 667, India

CORRESPONDING AUTHOR: ASHISH SINGH (e-mail: ashishnit07@gmail.com).

This work was supported by the Science and Engineering Research Board, Department of Science and Technology, Government of India (GoI), New Delhi, through the Core Research Grant Scheme (File No.: CRG/2021/000780/ES).

ABSTRACT The sub-threshold regime is suited for applications requiring ultra-low power consumption with low to medium frequency (tens to hundreds of MHz) of operation. Therefore, this paper presents electrical modeling and comprehensive analysis of copper-carbon nanotube (Cu-CNT) composite interconnects for sub-threshold circuit design. At lower operating frequencies, the effective complex conductivity of Cu-CNT composites in the nanoscale is formulated by developing an analytical model. Based on the proposed equivalent single conductor model, the frequency-dependent resistance and inductance of composite interconnects are computed. Finally, the sub-threshold crosstalk effect, transfer gain, and Nyquist stability of coupled Cu-CNT composite interconnect are analyzed using *ABCD* matrix approach.

INDEX TERMS Cu–CNT composite, delay, effective conductivity, frequency response, relative stability, sub-threshold.

I. INTRODUCTION

Development of electronic devices is undergoing a paradigm shift with their continued miniaturization [1]. In the current research scenario, due to the exponential scaling of metal-oxide semiconductor (MOS) devices, global interconnect delay is becoming one of the major concerns. More importantly, the reliability issue has become a crucial issue faced by the integrated circuits (ICs) due to rapidly increasing current densities. At nanoscale technology nodes, mechanisms such as surface scattering and grain boundary scattering play a crucial role in the performance estimation of on-chip copper (Cu) interconnects [2], [3], [4]. Such effects are further aggravated below 10 nm since Cu ions start diffusing through Cu-dielectric interface and grain boundary along the interconnect length. This result in discontinuity and void in Cu lines, which leads to the electrical, mechanical, thermal performance degradation and reliability issues during the design of nano-packaging on-chip, interconnects [5]. Diffusion of Cu ions becomes prominent at lower technology nodes because activation energy is smaller than the bulk Cu. Diffusion of Cu ions into the dielectric region creates a leakage path between dielectric and metal layer and it also severely degrades the quality of the dielectric. Therefore, researchers have to look for alternative solutions to this issue.

In the last few decades, carbon nanotubes (CNTs) have attracted a lot of attention as next-generation interconnect technology [6], [7]. CNTs exhibit higher ampacity (maximum current-carrying capacity), larger thermal conductivity, and long mean free path due to their strong C–C bonding in comparison with copper (Cu) counterpart [8], [9], [10]. Thus, for applications mainly in the nanoscale regime, CNTs exhibit superior electrical performance than Cu. Previously, a composite of Cu-CNT was demonstrated in [11]. The fabricated results showed that the thermal conductivity of Cu-CNT composite (395 W m^{-1} K^{-1}) is comparable with Cu. The Cu-CNT composite possesses excellent compatibility with silicon due to a much-reduced coefficient of thermal expansion mismatch, which is ∼10%. More encouraging results

were shown by Subramaniam et al. [12]. They successfully fabricated Cu-CNT composite and demonstrated about 100 × higher ampacity over Cu. Without sacrificing reliability, the composite exhibits superior electrical characteristics with significantly high electromigration resistance and ∼13% reduced electrical conductivity. The Cu-CNT composite can be fabricated by electrodepositing Cu into the pores of premade CNTs. Using a two-stage electroplating and electroless plating process, Cu can then be interlaced into the CNTs [13]. The vertically aligned CNTs were also demonstrated in [14] using chemical vapor deposition and plasma-enhanced chemical vapor deposition techniques. In particular, the Cu-CNT composite is potential in achieving a better trade-off between the performance and reliability and can facilitate a more realistic approach for fabricating on-chip interconnects. However, an in-depth analysis of the sub-threshold performance of Cu-CNT composite based interconnects in ICs which require low to medium performance is still lacking. Our previous research work has successfully established the potential of CNT bundle for sub-threshold interconnects [15]. Thus, it seems reasonable to extend the analysis for Cu-CNT composites to meet the near-future challenges such as higher crosstalk delay and degraded reliability of sub-threshold interconnects, which is the main impetus behind this research study.

In this paper, different composites comprising of Cu-SWCNT bundle (Cu-SWB), Cu-MCWNT bundle (Cu-MWB), and Cu-mixed CNT bundle (Cu-MCB) are considered. The performance of different Cu-CNT composites is computed using Gaussian distribution criterion. It is illustrated that after co-depositing more number of CNTs with Cu, the conductivity of Cu-CNT composites is significantly increased. The electrical performance of Cu-CNT composite interconnects could also be improved by increasing the metallic fraction, as reported in [16], similar to the pure CNTs. The rest of this paper is organized as follows: In Section II, the electrical modeling and characterization of different composite bundles is described with the effective complex conductivity for each bundle computed accurately. Thereafter, a distributed equivalent single conductor (ESC) model of the sub-threshold operated, driver–interconnect–load (DIL) system is presented and the frequency dependent interconnect impedance elements are evaluated for Cu-SWB and Cu-MWB composites in 16 nm technology node. In Section III, using *ABCD* technique, the performance characterization of CMOS inverter driven three line coupled Cu-CNT composites in sub–threshold regime is presented. The Cu-CNT bundled interconnects are analyzed in terms of sub–threshold crosstalk delay, frequency response, and Nyquist stability. The design parameters such as CNT filling ratio, metallic fraction of CNTs within the composite, length, and switching factors are considered. Finally, conclusions are drawn in Section IV.

II. ELECTRICAL MODEL OF COPPER-CNT COMPOSITES

The schematic of a pair of Cu-CNT composites placed at a distance d over the ground plane is shown in Fig. 1(a). The cross-sectional area of the bundle is considered as 18 nm × 54 nm with an aspect ratio of 3:1. Further, w, t, and l symbolize the width, thickness, and length of the bundle, respectively. The Cu-CNT composite consists of G types of CNTs having non-uniform diameters with an inter-shell spacing of $\delta = 0.34$ nm. In this analysis, ten different types of CNTs are taken into consideration i.e., $G = 10$ whose diameter D ranges from $D_1 \leq D_i \leq D_{\max}$ where, $D_1 = 1$ nm and $D_{\max} = 7.12$ nm, are the inner and outer shell diameter of MWCNT, respectively.

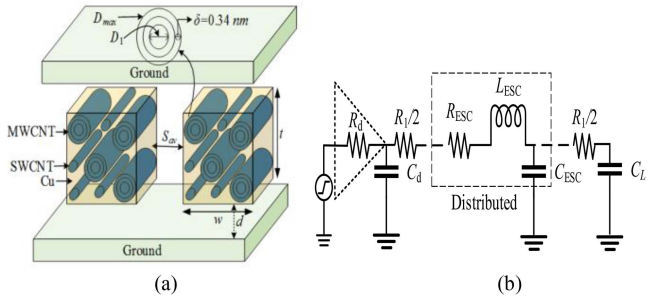

FIGURE 1. (a) Schematic view and (b) Distributed equivalent single conductor (ESC) model of Cu-SWB/ Cu-MWB/ Cu-MCB composite interconnects.

The diameter D_i of the i^{th} shell of MWCNT is given as $D_i = D_1 + 2 \cdot \delta \cdot (i-1)$, where, $1 \leq i \leq m$

$$\text{Also, } D_1 = \left(D'_{\text{out}} - 3\sigma_{D_{\text{out}}}\right) \text{ and } G = 3\sigma_{D_{\text{out}}}/\delta \tag{1}$$

In (1), m, D'_{out} and $\sigma_{D_{out}}$ represent the number of shells of MWCNT, the mean diameter and standard deviation, respectively. The CNT filling ratio, f_{cnt} is defined as the fraction of CNTs to total bundle area and is given by [17]

$$f_{\text{cnt}} = N_{\text{c}}\pi(D_{\max} + 0.31 \text{ nm})^2/4wt \tag{2}$$

where, N_{c} is the total number of CNTs inside the composite bundle. Moreover, a spacing of 0.155 nm between Cu and carbon atoms is taken into account in the model [18]. For realistic analysis, the CNT diameters inside the Cu-CNT composite have been considered to follow Gaussian distribution which is also consistent with [19]. Thus, there is a possibility that CNT diameters lie within the range $(D'_{out} - 3\sigma_{D_{out}})$ to $(D'_{out} + 3\sigma_{D_{out}})$. For the given mean diameter and standard deviation, the number of CNTs having an outer diameter D_{out} in the bundle are obtained as [20]

$$N(D_{\text{out}}) = \frac{N_{\text{c}} \times f_{\text{cnt}}}{\sigma_{D_{\text{out}}}\sqrt{2\pi} \times \left(D'^2_{\text{out}} + \sigma^2_{D_{\text{out}}}\right)} \times e^{-\left[\frac{1}{2}\left(\frac{D_{\text{out}} - D'_{\text{out}}}{\sigma_{D_{\text{out}}}}\right)^2\right]} \tag{3}$$

For the cross-sectional area of 18 nm × 54 nm, mean diameter and standard deviation considered are 3.71 nm and 1.13 nm, respectively. The distribution of CNTs in Cu-SWB, Cu-MWB, and Cu-MCB composites for different f_{cnt} is presented in Table 1. The probability of distribution of CNTs in Cu-MCB composite having a particular diameter D_i in the range 1 nm to 7.12 nm with $f_{\text{cnt}} = 0.2$ and 0.5 is illustrated in Table 2.

TABLE 1. Number of CNTs Corresponding to Filling Ratio in Cu-SWB, Cu-MWB and Cu-MCB Composites

f_{cnt}	Cu-SWB	Cu-MWB	Cu-MCB	
	Number of SWCNTs	Number of MWCNTs	Number of SWCNTs	Number of MWCNTs
0.2	44	18	22	11
0.3	60	25	30	19
0.4	79	34	43	27
0.5	95	47	54	35
0.6	112	60	65	44

TABLE 2. Number of CNTs and Corresponding Diameters in Cu-MCB

Diameter D_i (nm)	$f_{cnt} = 0.2$		$f_{cnt} = 0.5$	
	No. of SWCNTs	No. of MWCNTs	No. of SWCNTs	No. of MWCNTs
1.00	18	0	48	0
1.68	3	0	5	1
2.36	1	1	1	2
3.04	0	1	0	4
3.72	0	1	0	8
4.40	0	1	0	5
5.08	0	1	0	7
5.76	0	1	0	3
6.44	0	3	0	2
7.12	0	2	0	3

A. EFFECTIVE COMPLEX CONDUCTIVITY MODEL OF CU-CNT COMPOSITES AND THEIR COMPARISON

The effective complex conductivity, σ_{eff} of Cu-CNT composite bundle can be computed as [17]

$$\sigma_{\text{eff}} = (1 - f_{\text{cnt}})\,\sigma_{\text{Cu}} + f_{\text{cnt}}\sigma_{\text{cnt}} \tag{4}$$

where, σ_{cnt} is the CNT conductivity and σ_{Cu} is the conductivity of Cu. The value of σ_{cnt} can be computed by [17]

$$\sigma_{\text{cnt}} = k_c / Z_{\text{cnt}} \text{ with } k_c = F_m 4 \cdot l / \pi (D_{\text{out}} + 0.31\,\text{nm})^2 \tag{5}$$

Here, Z_{cnt} is the intrinsic impedance of an isolated CNT and F_m is the metallic fraction of CNTs inside the bundle. The value of F_m for the case of Cu-MWB composite is 1. For a shell of MWCNT or an SWCNT, the intrinsic self-impedance Z_{SWCNT} is determined by [21]

$$Z_{\text{SWCNT}} = R_{c,\text{ESC}} + \frac{h}{4e^2}\frac{l}{N_{\text{ch},i}}\left(\frac{1}{\lambda_{\text{mfp},i}} + \frac{j\omega}{v_F}\right) \tag{6}$$

where, $R_{c,\text{ESC}}$ is the imperfect contact resistance which depends largely on the fabrication technology, h is the Planck's constant, e is the electronic charge, $N_{\text{ch},i}$ is the number of conducting channels of the i^{th} shell of an isolated CNT, ω is the angular frequency, $\lambda_{\text{mfp},i}$ $(= 1000\,D_i)$ is the mean free path, and v_F symbolizes the Fermi velocity. Moreover, an MWCNT is the coaxial assembly of SWCNTs whose self-impedance Z_{MWCNT} is the parallel combination of each shell impedance. For m shells, it can be obtained by [21]

$$Z_{\text{MWCNT}} = \sum_{i=1}^{m} 1 / Z_{\text{SWCNT}}\,(D_i) \tag{7}$$

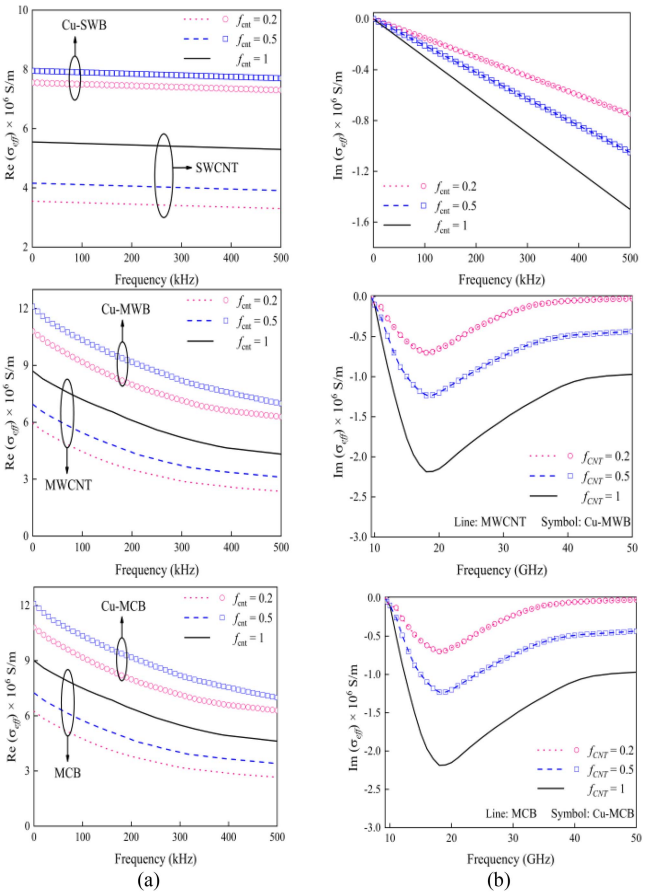

FIGURE 2. Effective complex conductivity of Cu-SWB, Cu-MWB, and Cu-MCB composite interconnects versus frequency (a) Real and (b) Imaginary conductivities for different filling ratios.

Substituting $Z_{\text{cnt}} = R_{\text{cnt}} + j\omega L_{\text{cnt}}$ and (5) into (4), we can obtain

$$\sigma_{\text{eff}} = (1 - f_{\text{cnt}})\,\sigma_{\text{Cu}} + \frac{k_c f_{\text{cnt}} R_{\text{cnt}}}{R_{\text{cnt}}^2 + \omega^2 L_{\text{cnt}}^2} - j\frac{k_c f_{\text{cnt}} \omega L_{\text{cnt}}}{R_{\text{cnt}}^2 + \omega^2 L_{\text{cnt}}^2} \tag{8}$$

where, R_{cnt} and L_{cnt} denote the resistance and inductance of an isolated CNT.

The performance of different composite bundles is investigated in terms of σ_{eff} and is compared with the pure CNT counterparts in Fig. 2. From Fig. 2(a), it is observed that Re (σ_{eff}) of Cu-SWB and its pure CNT counterpart remains constant with increase in frequency. This is because for SWCNTs, R_{cnt} is much larger than its reactance ωL_{cnt}. For Cu-MWB, Cu-MCB, and their pure CNT counterparts, R_{cnt} decreases with increase in the number of shells due to the increased $\lambda_{\text{mfp},i}$. Hence, with increase in frequency, the term ωL_{cnt} dominates over R_{cnt} and Re (σ_{eff}) drops at high frequencies. For the case of Cu-SWB and Cu-MWB composites, Re (σ_{eff}) at $f = 100$ kHz, is improved by 29% and 37%, respectively as f_{cnt} is increased from 0.2 to 0.5. Therefore, the electrical conductivity improves remarkably after co-depositing more number of CNTs with Cu in the nanoscale regime. The break frequency from (8) is calculated as $R_{\text{cnt}}/2\pi L_{\text{cnt}}$. For 16 nm

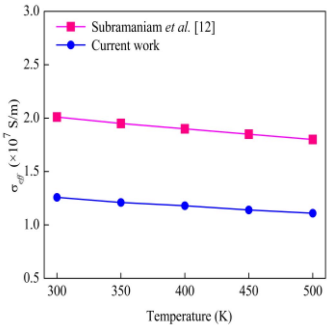

FIGURE 3. Effective conductivity of Cu-MCB versus temperature and its comparison with the experimental results reported in [12].

technology node, the values of R_{cnt} and L_{cnt} for MWCNT are computed as 5.91 kΩ and 49.2 nH whereas for SWCNT, these values are 9.85 kΩ and 6.31 pH, respectively. Thus, break frequency for MWCNTs is equal to 19.2 GHz, whereas for SWCNT, $R_{\text{cnt}}/2\pi L_{\text{cnt}}$ is equal to 248.7 GHz (Fig. 2(b)). In Fig. 2(b), only decreasing behaviour of Im (σ_{eff}) is observed where the highest frequency plotted is 500 kHz due to sub-threshold operation.

Im (σ_{eff}) of Cu-CNT composite also exhibits a similar trend to that of the corresponding CNT, as it is dependent on f_{cnt} only and increases with f_{cnt} at a particular frequency. Moreover, due to their similar electrical properties, Re (σ_{eff}) and Im (σ_{eff}) of Cu-MWB and Cu-MCB composites are almost identical and thus, Cu-MCB composites are not included in the following analysis. Moreover, σ_{eff} of Cu-MCB for $f_{\text{cnt}} = 0.5$ is validated with the experimental results of [12] and is shown in Fig. 3. It is observed that σ_{eff} of Cu-MCB composites closely resembles the measured data and the error may be attributed to the different alignment of CNTs.

B. EQUIVALENT SINGLE CONDUCTOR MODEL

The sub-threshold driver-interconnect-load (Sub-DIL) system incorporating an equivalent single conductor (ESC) model is shown in Fig. 1(b). The CMOS inverter acts as driver and sub-threshold drain current, for rising ramp input voltage is represented by [22], [23]

$$I_{\text{d}} = \mu_{\text{n}} C_{\text{ox}} \frac{W}{L} (\eta - 1) V_{\text{th}}^2 \cdot \exp\left(V_{\text{in}} - V_T / \eta V_{\text{th}}\right) \cdot \left[1 - \exp\left(-V_{\text{ds}} / V_{\text{th}}\right)\right] \tag{9}$$

In (9), μ_{n} is the electron mobility, C_{ox} is the gate-oxide capacitance per unit area, W and L are the effective channel width and channel length respectively, V_{th} is the thermal voltage, V_{T} is the threshold voltage, V_{in} and V_{ds} are the input voltage and drain-to-source voltage respectively and η is the sub-threshold slope factor whose value lies between one and two. Under high values of V_{ds} much greater than V_{th}, the factor $[1 - \exp(-V_{ds}/V_{th})]$ in (9) is close to unity. I_{d} thus becomes independent of V_{ds} and driver is treated saturated. On the other hand, under low values of V_{ds} much lower than V_{th}, the term $[1 - \exp(-V_{ds}/V_{th})]$ in (9) can be truncated to the first order Taylor series. Thus, I_{d} is proportional to V_{ds} and driver behaves as a linear resistor. Summarizing, the drain current in these two regions can be expressed as

$$I_{\text{d}} = \begin{cases} B_{\text{n}} \cdot \exp\left(\frac{V_{\text{in}} - V_{\text{T}}}{\eta V_{\text{th}}}\right) & \text{for } V_{\text{ds}} \geq 4V_{\text{th}} \\ \gamma_{\text{n}} \cdot V_{\text{ds}} & \text{for } V_{\text{ds}} < 4V_{\text{th}} \end{cases} \tag{10}$$

In (10), the values of B_{n} in sub-saturation region and γ_{n} in sub-linear region are given as

$$B_{\text{n}} = \mu_{\text{n}} C_{\text{ox}} \left(W/L\right) (\eta - 1) V_{\text{th}}^2 \tag{11}$$

$$\gamma_{\text{n}} = \mu_{\text{n}} C_{\text{ox}} \frac{W}{L} (\eta - 1) V_{\text{th}} \tag{12}$$

The process parameters in (10) as obtained from 16 nm BSIM Level-54 CMOS model file are: $\mu_{\text{n}} = 0.03$ m^2/ V-s, $t_{\text{ox}} = 0.95$ nm, $\eta = 2$. On substituting these values, the driver resistance in sub-threshold region is computed as $R_{\text{d}} = 1/\gamma_{\text{n}} = 21.8$ kΩ.

Next, the parasitics of Cu-CNT composite interconnect as such are dependent on the number of conducting channels $N_{\text{ch},i}$ and are function of the CNT diameter of the i^{th} shell, given as

$$N_{\text{ch},i}(D_i) = \begin{cases} x_1 T D_i + x_2 & D_i > d_T/T \\ 2/3 & D_i \leq d_T/T \end{cases} \tag{13}$$

where, $x_1 = 0.116$ and $x_2 = 0.21$, and d_T is 1300 nm · K at $T =$ 300 K. In the ESC model of Cu-CNT composite interconnect, imperfect contact resistance, $R_{c,\text{ESC}}$ and quantum resistance, R_q ($= h/4e^2$) behave as its lumped component (R_1) [17] as

$$R_1 = \frac{f_{\text{cnt}}}{N_{\text{c}}} \times \left(R_{c,\text{ESC}} + \frac{h}{4e^2 N_{\text{ch},i}}\right) \tag{14}$$

In addition, the equivalent scattering resistance (R_{ESC}) behaves as distributive component and is dependent on Re (σ_{eff}). The per unit length (*p.u.l.*) R_{ESC} for Cu-CNT composite interconnect is determined by

$$R_{\text{ESC}} = \frac{\rho_{\text{eff}}}{wt} = \text{Re}\left(\frac{1}{\sigma_{\text{eff}}}\right) \frac{1}{w \cdot t} \tag{15}$$

where, $\rho_{\text{eff}} = \text{Re}\,(1/\,\sigma_{\text{eff}})$ is the effective complex resistivity. The inner and external inductances of Cu-CNT interconnect determine its *p.u.l* inductance (L_{ESC}), given as [10]

$$L_{\text{ESC}} = L_{\text{in}} + L_{\text{ext}} = \text{Im}\left(\frac{1}{\sigma_{\text{eff}}} \frac{1}{wt}\right) + \frac{\mu_0 \varepsilon_0 \varepsilon_r}{C_{e,\text{ESC}}} \tag{16}$$

where, μ_0 and ε_0 are the permeability and permittivity in vacuum, ε_r is the relative permittivity of the dielectric, and $C_{e,\text{ESC}}$ is the *p.u.l.* electrostatic capacitance that appears between the bundle and the ground plane, given as [17]

$$\frac{C_{e,\text{ESC}}}{\varepsilon_0 \varepsilon_r} = \frac{w}{d} + \frac{4}{\pi} \ln\left(1 + \frac{t}{d}\right) + \frac{6}{\pi} + \frac{2}{\pi} \ln\left[1 + \frac{\pi w}{2(1+\pi)(t+d)}\right] \tag{17}$$

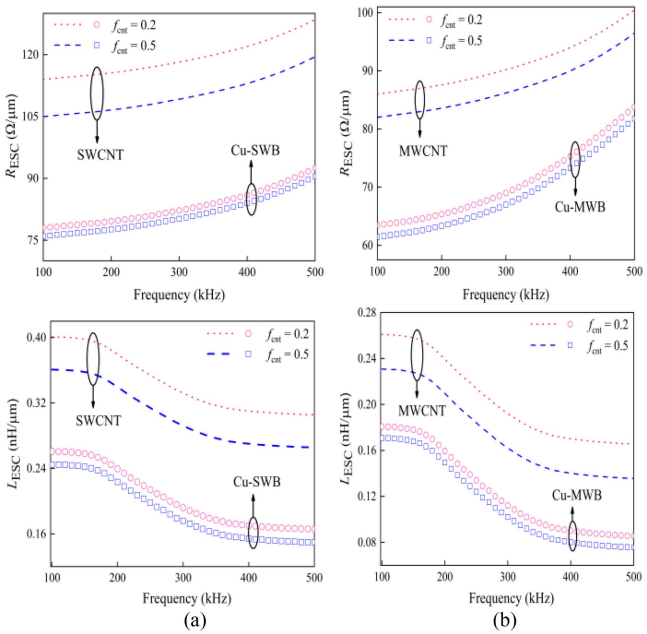

FIGURE 4. **(a) Per unit length R_{ESC} and L_{ESC} of (a) Cu-SWB/ SWCNT and (b) Cu-MWB/ MWCNT versus frequency for different f_{cnt} ratios.**

The *p.u.l.* quantum capacitance due to quantum electrostatic energies stored inside the channel of CNTs are calculated as

$$C_{q,\mathrm{ESC}} = \left(4e^2 N_c / h v_F\right) \times \sum_{i=1}^{m} N_{\mathrm{ch},i} \tag{18}$$

The total *p.u.l.* equivalent capacitance C_{ESC} is expressed as

$$C_{\mathrm{ESC}} = \left(1/C_{e,\mathrm{ESC}} + 1/C_{q,\mathrm{ESC}}\right)^{-1} \tag{19}$$

Based on (4)–(19), the frequency dependent resistance and inductance of Cu-SWB and Cu-MWB composite interconnects is extracted in Fig. 4 for different f_{cnt} values. The bundle length is set to be 100 μm. Here, it is seen that co-depositing SWCNTs and/or MWCNTs with Cu significantly suppresses the resistance and inductance of the composite bundled interconnects over isolated CNTs. Moreover, with increase in f_{cnt}, R_{ESC} and L_{ESC} of Cu-SWB and Cu-MWB composites decreases, thus resulting in better electrical performance. For a certain value of f_{cnt}, the Cu-MWB composite interconnect exhibits a lower resistance as well as inductance in comparison to the Cu-SWB and isolated CNTs. The reason for this phenomenon is attributed to the presence of significantly larger kinetic inductance in MWCNTs, which is ~two orders larger than the magnetic inductance, or in other words, due to large momentum relaxation time in MWCNTs.

III. PERFORMANCE ANALYSIS

A. CROSSTALK EFFECT

In this section, the prominent crosstalk issue arising in sub-threshold composite Cu-CNT interconnects is examined. The

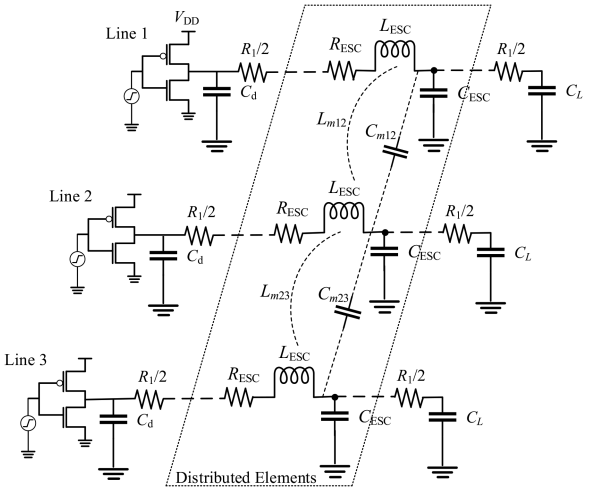

FIGURE 5. **Distributed ESC model of coupled three-line Cu-CNT composite interconnects.**

equivalent circuit of three coupled Cu-CNT composite interconnect employing sub-DIL system is shown in Fig. 5. In the Sub–DIL coupled system, lines 1, 3 serve as the aggressor and line 2 as victim. The signal transmission in coupled composite interconnects can be classified into in-phase and out-phase. The two phase modes are defined as k_1 and k_2 where $k_1 = 1$, $k_2 = -1$ under out-phase and $k_1 = k_2 = +1$ under in-phase. The *ABCD* matrix for the victim sub–threshold composite interconnects is given as [24]

$$\begin{bmatrix} A & B \\ C & D \end{bmatrix} = \begin{bmatrix} 1 + sC_dR_d & R_d \\ sC_d & 1 \end{bmatrix} \begin{bmatrix} 1 & R_1/2 \\ 0 & 1 \end{bmatrix} \times \begin{bmatrix} \cosh(\theta l) & Z_0 \sinh(\theta l) \\ \sinh(\theta l)/Z_0 & \cosh(\theta l) \end{bmatrix} \begin{bmatrix} 1 & R_1/2 \\ 0 & 1 \end{bmatrix} \tag{20}$$

$$\text{and } \theta = \frac{\sqrt{\left[R_{\mathrm{ESC}} + s\left(L_{\mathrm{ESC}} + k_1 L_{m12} + k_2 L_{m23}\right)\right] sC_{\mathrm{ESC}} \Delta x}}{(\Delta x)} \tag{21}$$

$$Z_0 = \sqrt{\frac{R_{\mathrm{ESC}} + s\left(L_{\mathrm{ESC}} + k_1 L_{m12} + k_2 L_{m23}\right)}{s\left(C_{\mathrm{ESC}} + (1-k_1) C_{m12} + (1-k_2) C_{m13}\right)}} \tag{22}$$

where, θ and Z_0 represent the propagation constant and characteristic impedance, respectively, L_m and C_m denote the mutual inductance and capacitance, Δx is the infinitesimal segment in the ESC model, and C_d is the drain diffusion capacitance.

The 50% time delay of victim Cu-CNT composite line is obtained by [25]

$$\tau_{50\%} = \left(1.48\xi + e^{-2.9\xi^{1.35}}\right) \sqrt{L_{\mathrm{equ}} l \left(C_{\mathrm{equ}} l + C_L\right)} \tag{23}$$

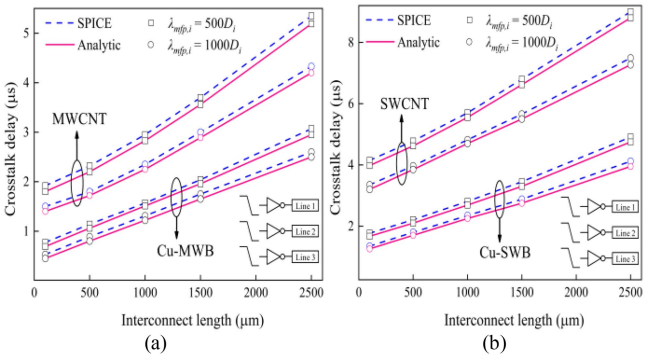

FIGURE 6. Sub-threshold crosstalk delay of (a) Cu-MWB and (b) Cu-SWB composite interconnects for $\lambda_{mfp,i} = 1000D_i$ and $\lambda_{mfp,i} = 500D_i$.

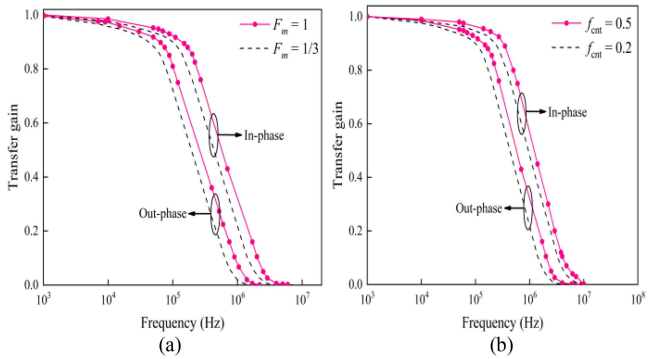

FIGURE 7. Frequency response curves of (a) Cu-SWB with $F_m = 1$, 1/3 and (b) Cu-MWB with $f_{cnt} = 0.2$, 0.5, under in-phase and out-phase.

where, C_L is the load capacitance, and equivalent resistance R_{equ}, inductance L_{equ}, capacitance C_{equ} of the decoupled victim line are determined as

$$\begin{aligned} R_{equ} &= R_{ESC} \\ L_{equ} &= L_{ESC} + k_1 L_{m12} + k_2 L_{m23} \\ C_{equ} &= C_{ESC} + (1 - k_1) C_{m12} + (1 - k_2) C_{m23} \end{aligned} \tag{24}$$

Here, C_{m12}, C_{m23} and L_{m12}, L_{m23} represent coupling capacitance and mutual inductances between the aggressor and victim lines. The coupling capacitance and mutual inductance can be obtained using expression [26], [27]

$$C_m = \pi \varepsilon_0 \varepsilon_r / \cosh^{-1}\left(S_p / D_1\right) \tag{25}$$

$$L_m = \mu_0 \varepsilon_0 / N_T C_e \tag{26}$$

where, S_p is the spacing between two coupled interconnects, N_T is the total number of tube counts, C_e is the electrostatic capacitance of CNTs facing the ground plane. For Cu-CNT composites, the value of C_{m12} and C_{m23} is found to be 1.55 fF. This is because C_{m12} depends upon the spacing between the interconnect lines which is same in Cu-MWB/Cu-MCB/Cu-SWB. The values of L_{m12} (L_{m23}) for Cu-MCB, Cu-MWB and Cu-SWB is determined to be 2.01 pH, 3.16pH and 3.57pH respectively, for $f_{cnt} = 0.5$. Here, ξ is the damping factor which can be expressed as

$$\xi = \frac{R_{equ} l \left(C_{equ} l + 2C_L\right) + 2\left(R_1 + R_d\right)\left(C_{equ} l + C_L\right)}{4\sqrt{L_{equ} l \left(C_{equ} l + C_L\right)}} \tag{27}$$

Fig. 6 presents the sub–threshold delay performance of Cu-CNT composite and pure CNT interconnects. Here, for SWCNTs, $F_m = 1/3$, while $f_{cnt} = 0.5$. Moreover, $R_d = 21.8$ kΩ, $C_d = 1$fF, and $C_L = 1$fF, while the relative permittivity, ε_r of dielectric is taken as 2. It is evident that Cu-CNT composite interconnects show reduced sub–threshold crosstalk delay than their pure CNT counterparts due to their much improved conductivity. Moreover, the sub-threshold delays of Cu-MWB/ Cu-SWB interconnects even with one-half of the mean free path i.e., $\lambda_{mfp} = 500D$ are relatively less influenced as compared with pure SWCNTs and MWCNTs. Hence, with defective CNTs having a dramatically reduced λ_{mfp}, the composite interconnects still demonstrate comparable sub-threshold delay with that for $\lambda_{mfp} = 1000D$. On the basis of bundle arrangements in Fig. 6(b), it is noticed that in comparison to Cu-SWB, since Cu-MWB has more number of conducting channels, therefore, it exhibits a reduced delay due to reduction in the equivalent resistance, inductance and capacitance values. The percentage improvements in the crosstalk delay for Cu-MWB compared to MWCNT for $\lambda_{mfp} = 1000D$ are 67.81%, 45.55%, and 20.12% at 100-, 1000- and 2500 μm lengths, respectively. The analytical results also match closely with the simulation results.

B. TRANSFER GAIN

The input-to-output transfer function $G(s)$ from (22) is

$$\begin{aligned} G(s) &= \frac{1}{A + sC_L B} \\ &= \begin{bmatrix} (1 + sR_d (C_d + C_L)) \cosh(\theta l) \\ + \left(Z_0 R_d + sZ_0 C_L + s^2 Z_0 C_d C_L R_d\right) \sinh(\theta l) \end{bmatrix}^{-1} \end{aligned} \tag{28}$$

Using the precise fourth-order Pade's approximation, the transfer function $G(s)$ from (28), can be written as

$$G(s) \approx \left[1 + c_1 s + c_2 s^2 + c_3 s^3 + c_4 s^4\right]^{-1} \tag{29}$$

The coefficients c_1, c_2, c_3, and c_4 depend on the parameters of sub-DIL system and can be referred in [15]. The effect of metallic fraction variation on the frequency response of three coupled Cu-SWB composite interconnects under in-phase ($k_1 = k_2 = 1$) and out-phase ($k_1 = 1$, $k_2 = -1$) switching modes is presented in Fig. 7(a). The interconnect spacing is chosen to be 18 nm and the bundle length considered is $l = 100$ μm. The expression $R_{equ}/(2\pi L_{equ})$ is utilized to compute the cut-off frequency, f_c. Since the number of conducting channels are lesser in the Cu-SWB composite with $F_m = 1/3$, the total inductance is $\times 3$ times larger than a densely packed bundle with $F_m = 1$, whereas their capacitances remain virtually unchanged. Therefore, the parasitics R_{equ} and C_{equ} associated with Cu-SWB composite interconnect for $F_m = 1$ are lower and hence, it exhibits an f_c of 0.79 MHz, while f_c in the case

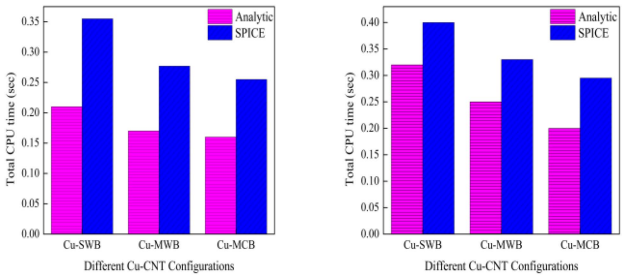

FIGURE 8. Total CPU time versus different Cu-CNT configurations under (a) in-phase and (b) Out-phase.

TABLE 3. Rise Time and Percentage Overshoot in Cu-MWB for Various Filling Ratios and Fraction of Metallic CNTs

Design metric	Value	T_r (in μs) for		$\%\ M_p$ for	
		l = 10 μm,	l =1000 μm	l = 10 μm,	l = 1000 μm
Filling ratio	0.3	0.545	957	14.08	0
	0.4	0.472	906	22.35	0
	0.5	0.396	853	28.89	0
Probability	1	0.178	694	42.65	0
	1/3	0.285	705	37.86	0

of $F_{\mathrm{m}} = 1/3$ is 0.75 MHz under in-phase switching. Hence, the frequency response can be improved by increasing F_{m} due to the decreased mutual inductance. Similar variations are also observed under out-phase switching mode. As CNTs with filling ratio of 0.2 were reported in [21], the influence of f_{cnt} on the frequency response of coupled Cu-MWB interconnects is studied in Fig. 7(b). The values of f_{c} exhibited by Cu-MWB for $f_{\mathrm{cnt}} = 0.2$ and $f_{\mathrm{cnt}} = 0.5$ are 0.91 MHz and 0.94 MHz under in-phase switching. This is so because increasing f_{cnt} improves the Cu-MWB effective conductivity, and thereby improves the cut-off frequency or bandwidth. Furthermore, the effective capacitance for ($k_1 = k_2 = 1$) mode is much smaller compared to the ($k_1 = 1, k_2 = -1$) due to the Miller effect, i.e., $C_{\mathrm{ESC}} << C_{\mathrm{ESC}} + 2C_{m23}$. Hence, the values of f_{c} exhibited by the Cu-MWB and Cu-SWB composite interconnects under out-phase switching are reduced compared to that under in-phase.

Subsequently, comparison of CPU time to compute in-phase and out-phase sub-threshold delays for different Cu-CNT composite configurations using the proposed analytical model and SPICE simulations is shown in Fig. 8.

C. NYQUIST STABILITY OF COMPOSITE BUNDLES IN SUB–THRESHOLD

A DIL system is said to be stable if its rise time, T_r is higher and peak overshoot voltage, M_p is zero. The T_r and M_p mainly depend on the damping coefficient as presented in (29). In this analysis, SWCNT and MWCNT diameter ranging from 1 nm-2.76 nm and 1 nm-7.12 nm, respectively are taken into account. The quantitative values of T_r and M_p for different filling ratios and metallic fraction of CNTs for Cu-MWB composite are summarized in Table 3. Based on the transfer function $G(s)$ in (30), the Nyquist plots of Cu-MWB composite interconnect wherein length is varied from 10 $\mu\mathrm{m} \leq l \leq 100$ μm, are shown in Fig. 9(a). Based on stability theory, farther the encirclement moves away from the critical point (–1, 0) in complex plane, more the system tends towards stability. It can be observed that by increasing the length of Cu-MWB composite, the critical point (–1, 0) goes towards outside the Nyquist plot and the system becomes more stable. Similarly, in Fig. 9(b), Nyquist diagram shows the impact on relative stability against variations in the filling ratio from $0.3 \leq f_{\mathrm{cnt}} \leq 0.5$. With the increase in f_{cnt} value, $N_{\mathrm{ch},i}$ increases, which in turn improves σ_{eff} and increases the C_{ESC} of Cu-MWB composite interconnect. Note that C_{ESC} is the governing parameter in determining T_r, and with rise in the values of either $C_{\mathrm{e,ESC}}$ and $C_{\mathrm{q,ESC}}$ of Cu-MWB, the DIL system tends to damp more promptly, and the system becomes stable.

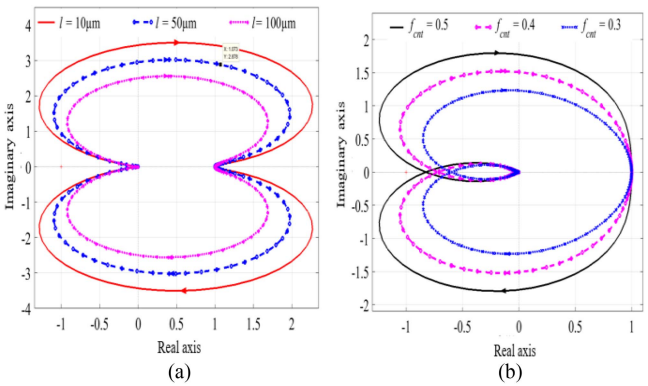

FIGURE 9. Nyquist plots for coupled Cu-MWB composite sub-DIR system for (a) 10 μm $\leq l \leq$ 1000 μm and (b) 0.3 $\leq f_{\mathrm{cnt}} \leq$ 0.5.

IV. CONCLUSION

The novel research work carried out in this paper shows the applicability of three different Cu-CNT composites i.e., Cu-SWB/Cu-MWB/and Cu-MCB as interconnects through modeling, simulation and analysis under the sub–threshold region. Using Gaussian distribution, the number of CNTs in Cu-CNT composites is derived. Thereafter, the distributed equivalent single conductor model for composite interconnects is developed. The effective complex conductivity of composites for different filling ratios at much lower operating frequencies is extracted by developing mathematical formulations. It is found that Cu-MWB composite has a larger conductivity than that of the Cu-SWB. For certain f_{cnt}, the frequency dependent resistance as well as inductance of Cu-MWB composite interconnects are much lower than Cu-SWB and isolated CNT counterparts.

By the virtue of equivalent single conductor model, the sub-threshold performance is computed for three line coupled Cu-SWB/ Cu-MWB composite interconnects through analytical *ABCD* technique and SPICE simulations. It is determined that Cu-MWB leads to improved electrical conductivity, reduced crosstalk, higher bandwidth, and stability and thus, shall be a better choice amongst other composite bundles and pure CNTs. The analytical results also match closely with the

simulation results. Hence, it is concluded that at present time, Cu-MWB can be observed as a feasible solution to meet the near future challenges of on-chip sub-threshold interconnects. The results of our investigations shall be highly lucrative in the realization of Cu-MWB composite interconnects for sub-threshold ICs and can open up a new era for ultra–low power circuits.

ACKNOWLEDGMENT

The authors would also like to thank the Science and Engineering Research Board, Department of Science and Technology, GoI, New Delhi for technical support.

REFERENCES

[1] U.S. Congress, Office of Technology Assessment, *Miniaturization Technologies*, OTA-TCT-514, Washington, DC, USA: U.S. Government Printing Office, Nov. 1991.
[2] G. Lopez, J. Davis, and J. Meindl, "A new physical model and experimental measurements of copper interconnect resistivity considering size effects and line-edge roughness (LER)," in *Proc. IEEE Int. Interconnect Technol. Conf.*, 2009, pp. 231–234.
[3] S. Kumar and R. Sharma, "Analytical model for resistivity and mean free path in on-chip interconnects with rough surfaces," *IEEE Trans. Emerg. Topics Comput.*, vol. 6, no. 2, pp. 233–243, Apr.–Jun. 2018.
[4] "IEEE international roadmap for devices and systems report," 2017. [Online]. Available: https://irds.ieee.org/roadmap-2017
[5] W. Zhang et al., "Influence of the electron mean free path on the resistivity of thin metal films," *Microelectronic Eng.*, vol. 76, no. 1–4, pp. 146–152, Oct. 2004.
[6] H. Li, C. Xu, N. Srivastava, and K. Banerjee, "Carbon nanomaterials for next-generation interconnects and passives: Physics, status, and prospects," *IEEE Trans. Electron Devices*, vol. 56, no. 9, pp. 1799–1821, Sep. 2009.
[7] M. Gholipour and N. Masoumi, "Efficient inclusive analytical model for delay estimation of multi-walled carbon nanotube interconnects," *IET Circuits Devices Syst.*, vol. 6, no. 4, pp. 252–259, 2012.
[8] J. Y. Park et al., "Electron-phonon scattering in metallic single-walled carbon nanotubes," *Nano Lett.*, vol. 4, no. 3, pp. 517–520, 2004.
[9] A. Kumar and B. K. Kaushik, "Transient analysis of hybrid Cu-CNT on-chip interconnects using MRA technique," *IEEE Open J. Nanotechnol.*, vol. 3, pp. 24–35, 2022.
[10] V. R. Kumar, B. K. Kaushik, and A. Patnaik, "Improved crosstalk noise modeling of MWCNT interconnects using FDTD technique," *Microelectron. J.*, vol. 46, no. 12, pp. 1263–1268, Dec. 2015.
[11] C. Subramaniam et al., "Carbon nanotube-copper exhibiting metal-like thermal conductivity and silicon-like thermal expansion for efficient cooling of electronics," *Nanoscale*, vol. 6, pp. 2669–2674, 2014.
[12] C. Subramaniam et al., "One hundred fold increase in current carrying capacity in a carbon nanotube–copper composite," *Nature Commun.*, vol. 4, pp. 1–7, 2013.
[13] L. Ladani et al., "Fabrication of carbon nanotube/copper and carbon nanofiber/copper composites for microelectronics," *Mater. Today Commun.*, vol. 11, pp. 123–131, 2017.
[14] S. Sun et al., "Vertically aligned CNT-Cu nano-composite material for stacked through-silicon-via interconnects," *Nanotechnolgy*, vol. 27, 2016, Art. no. 335705.
[15] A. Singh and R. Dhiman, "Proposal and analysis of mixed CNT bundle for sub-threshold interconnects," *IEEE Trans. Nanotechnol.*, vol. 18, pp. 584–588, 2019.
[16] A. R. Harutyunyan et al., "Preferential growth of single-walled carbon nanotubes with metallic conductivity," *Science*, vol. 326, no. 5949, pp. 116–120, Oct. 2009.
[17] Z. Cheng et al., "Investigation of copper–carbon nanotube composites as global VLSI interconnects," *IEEE Trans. Nanotechnol.*, vol. 16, no. 6, pp. 891–900, Nov. 2017.
[18] Y. Matsuda, W. Q. Deng, and W. A. Goddard III, "Contact resistance for 'end-contacted' metal-graphene and metal-nanotube interfaces from quantum mechanics," *J. Phys. Chem. C*, vol. 114, pp. 17845–17850, 2010.
[19] W. S. Zhao et al., "High-frequency modeling of on-chip coupled carbon nanotube interconnects for multi-wave applications," *IEEE Trans. Compon. Packag. Manuf. Technol.*, vol. 6, no. 8, pp. 1226–1232, Aug. 2016.
[20] S. Haruehanroengra and W. Wang, "Analyzing conductance of mixed carbon-nanotube bundles for interconnect applications," *IEEE Electron. Device Lett.*, vol. 28, no. 8, pp. 756–759, Aug. 2007.
[21] W.-S. Zhao et al., "High-frequency analysis of Cu-carbon nanotube composite through-silicon vias," *IEEE Trans. Nanotechnol.*, vol. 15, no. 3, pp. 506–511, May 2016.
[22] A. Wang, B. H. Calhoun, and A. P. Chandrakasan, *Subthreshold Design for Ultra Low-Power Systems*. Berlin, Germany: Springer-verlag, 2006.
[23] M. Alioto, "Understanding DC behavior of subthreshold CMOS logic through closed-form analysis," *IEEE Trans. Circuits Syst. I: Regular Papers*, vol. 57, no. 7, pp. 1597–1607, Jul. 2010.
[24] M. Sahoo, P. Ghosal, and H. Rahaman, "Modeling and analysis of crosstalk induced effects in multiwalled carbon nanotube interconnects: An ABCD parameter-based approach," *IEEE Trans. Nanotechnol.*, vol. 14, no. 2, pp. 259–274, Mar. 2015.
[25] Y. I. Ismail and E. G. Friedman, "Effects of inductance on the propagation delay and repeater insertion in VLSI circuits," *IEEE Trans. Very Large Scale Integr. Syst.*, vol. 8, no. 2, pp. 195–206, Apr. 2000.
[26] M. K. Majumder, B. K. Kaushik, and S. K. Manhas, "Analysis of delay and dynamic crosstalk in bundled carbon nanotube interconnects," *IEEE Trans. Electromagn. Compat.*, vol. 56, no. 6, pp. 1666–1673, Dec. 2014.
[27] A. Kumar, V. R. Kumar, and B. K. Kaushik, "Transient analysis of crosstalk induced effects in mixed CNT bundle interconnects using FDTD technique," *IEEE Trans. Electromagn. Compat.*, vol. 61, no. 5, pp. 1621–1629, Oct. 2019.